nature structural & molecular biology

Dynein achieves processive motion using both stochastic and coordinated stepping

Weihong Qiu[1,8], Nathan D Derr[1–3,8], Brian S Goodman[1], Elizabeth Villa[4,5], David Wu[5,6], William Shih[2,3,7] & Samara L Reck-Peterson[1]

Processivity, the ability of single molecules to move continuously along a track, is a fundamental requirement of cargo-transporting molecular motors. Here, we investigate how cytoplasmic dynein, a homodimeric, microtubule-based motor, achieves processive motion. To do this, we developed a versatile method for assembling *Saccharomyces cerevisiae* dynein heterodimers, using complementary DNA oligonucleotides covalently linked to dynein monomers labeled with different organic fluorophores. Using two-color, single-molecule microscopy and high-precision, two-dimensional tracking, we find that dynein has a highly variable stepping pattern that is distinct from all other processive cytoskeletal motors, which use 'hand-over-hand' mechanisms. Uniquely, dynein stepping is stochastic when its two motor domains are close together. However, coordination emerges as the distance between motor domains increases, implying that a tension-based mechanism governs these steps. This plasticity may allow tuning of dynein for its diverse cellular functions.

© 2012 Nature America, Inc. All rights reserved.

The microtubule-based motor cytoplasmic dynein (referred to here as dynein) powers the transport of a diverse array of cargos, allowing cells to organize their contents, move, divide and respond to stimuli. Neurons and other long cells are especially sensitive to defects in transport; mutations in dynein motor-associated subunits lead to neurodevelopmental and neurodegenerative diseases[1,2]. Like other motors that move cargo over long distances, single dynein molecules move processively along their microtubule track[3–8]. Dynein is the last class of cytoskeletal motor for which the mechanism of processive motility remains unknown.

Dynein's mechanism continues to be mysterious because of its enormous size and complexity[9]. The dynein holoenzyme is composed of two ~500 kDa motor (or 'head') heavy chain subunits and at least six other polypeptides. The domain structure of the dynein heavy chain is shown in **Figure 1a**. The N-terminal 'tail' domain represents ~30% of the entire mass of the heavy chain and is required for dimerization and the interaction of most dynein subunits and associated proteins. Connected to the tail is the 'linker' domain, which is thought to amplify structural changes during dynein's ATPase cycle and is required for motility[5,10–12]. Following the linker domain are six concatenated AAA+ (ATPase associated with diverse cellular activities) domains, which fold into a ring. As a member of the AAA+ superfamily, dynein is evolutionarily distinct from kinesin and myosin, which are distantly related to G-proteins[13]. Dynein's first AAA+ domain is the primary site of ATP hydrolysis[14], but AAA+ domains 2–4 are also expected to bind ATP or ADP, based on mutant phenotypes[15–17]. Projecting from the fourth AAA+ domain is a 15 nm, antiparallel, coiled-coil 'stalk', capped by a globular microtubule-binding domain[18–20].

Despite the complexity of the dynein motor, a dimer of two truncated *S. cerevisiae* dynein heavy chains is sufficient for processive motility[5,21]. Previously, we showed that dynein monomers lacking most of the tail domain were not processive on their own but moved processively when they were linked together with glutathione *S*-transferase (GST, a stable homodimer)[5] (**Fig. 1b**). GST–dynein homodimers behaved similarly to native yeast dynein with respect to velocity, processivity, stepping behavior and force production *in vitro*[5,22], demonstrating that the native dimerization interface is not required for motility and suggesting that the basic motile mechanism is insensitive to the method of dimerization.

However, how dynein achieves processive motility remains unknown. For the well-studied kinesin-1 and myosin-V motors, nucleotide-driven conformational changes of their mechanical elements power the sequential hand-over-hand stepping of their two identical motor domains[23–27]. Previously, to investigate the dynein stepping mechanism, we labeled GST–dynein homodimers with a single quantum dot (Qdot) on a single motor domain or on the tail domain (approximate center of mass). High-precision one-dimensional stepping analyses revealed that the motor domain step size was nearly twice the size of the tail step size, consistent with a model in which dynein's two motor domains alternate their position in time and pass each other in space[5]. However, unlike kinesin,

[1]Department of Cell Biology, Harvard Medical School, Boston, Massachusetts, USA. [2]Dana Farber Cancer Institute, Boston, Massachusetts, USA. [3]Department of Biochemistry and Molecular Pharmacology, Harvard Medical School, Boston, Massachusetts, USA. [4]Department of Molecular Structural Biology, Max Planck Institute of Biochemistry, Martinsried, Germany. [5]Physiology Course, Marine Biological Laboratory, Woods Hole, Massachusetts, USA. [6]Geffen School of Medicine, University of California, Los Angeles, Los Angeles, California, USA. [7]Wyss Institute, Harvard University, Boston, Massachusetts, USA. [8]These authors contributed equally to this work. Correspondence should be addressed to S.L.R.-P. (reck-peterson@hms.harvard.edu).

Received 29 July 2011; accepted 18 November 2011; published online 8 January 2012; doi:10.1038/nsmb.2205

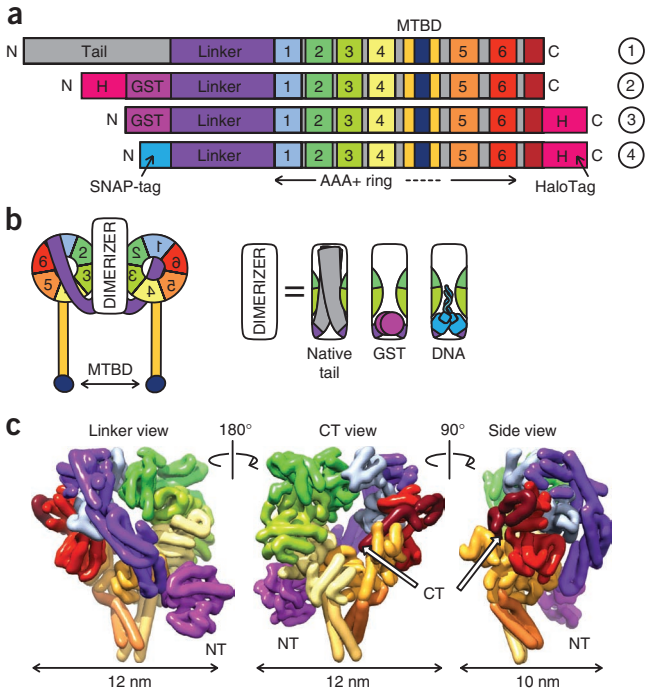

Figure 1 Dynein structure and constructs used in this study. (**a**) Linear diagrams of native dynein's domain structure (1) and constructs used in this study: GST-dimerized dynein with an N-terminal HaloTag (H) for tail-labeled experiments (2); GST-dimerized dynein with a C-terminal HaloTag for motor domain-labeled experiments (3); dynein monomer with an N-terminal SNAP-tag for DNA dimerization and a C-terminal HaloTag for motor domain labeling (4). MTBD, microtubule-binding domain. (**b**) Two-dimensional schematic of dimeric dynein. Dimerization (white box) can be achieved using the native protein dimerization domain, GST or complementary DNA oligomers attached through a SNAP-tag. (**c**) Three-dimensional structure of yeast dynein (PDB 3QMZ)[18], filtered to 8-Å resolution. Views from left to right: the linker face, the opposite face of the ring containing the C-terminal (CT) alpha helix, and the side of the ring. Dimerization is achieved through GST (magenta) at the N terminus (NT).

dynein takes steps of variable size and direction[4,5,8], making other stepping patterns theoretically possible[5]. Dynein's variable stepping behavior is probably due to its large size[10,12,28], which allows the motor rings to separate and access multiple microtubule binding sites. Although advances in understanding the architecture of the dynein motor domain have come from two near-atomic-resolution crystal structures[18,20] (**Fig. 1c**), how dynein's two motors are arranged on the microtubule when moving processively also remains unknown. Here, we set out to determine how dynein achieves processive motility.

A major barrier to determining the dynein stepping pattern and its structural basis is the lack of an efficient system to make high-affinity, functional heterodimers, so that each protomer can be probed independently. We created *S. cerevisiae* dynein heterodimers labeled with two distinct fluorophores through base-pairing of covalently attached, complementary DNA oligonucleotides. DNA-dimerized dynein behaved indistinguishably from native dynein and protein-based dynein homodimers[5,22]. Using two-color, single-molecule microscopy coupled with high-precision, two-dimensional particle tracking, we found that dynein has a highly unusual stepping pattern compared to processive kinesins and myosins. We show that dynein's two motor domains can step both alternately and non-alternately in time, and they can either pass or not pass each other in space. Unexpectedly, we found that many dynein steps are uncoordinated but become coordinated as the distance between the two motor domains increases. These results suggest that dynein can switch between stochastic and tension-based stepping, making it distinct from all other two-headed processive motors.

RESULTS

Two-dimensional analysis of dynein stepping

Because dynein's steps are known to have an off-axis component[5,8], analysis of stepping projected onto one dimension along the microtubule axis (as is standard in the field) could yield an underestimate of dynein's true step size. To determine the step size of dynein in two dimensions, we implemented a custom step-finding program (see **Supplementary Methods**). Before analyzing dynein's stepping behavior in two dimensions, we first determined the measurement precision of our total internal reflection fluorescence (TIRF) microscope to be ~1.5 nm for Qdot 655 and ~3.5 nm for the organic fluorophores Atto647N and Cy3B (**Supplementary Fig. 1a–c** and **Supplementary Methods**). As an additional control for the precision of our methods, we conducted one-dimensional and two-dimensional stepping experiments with the yeast kinesin-8 (Kip3)[29]. We found that kinesin-8 labeled on a single motor domain takes ~16-nm steps (**Supplementary Fig. 2a–d**), similarly to other kinesin family members[27].

To determine the two-dimensional step size of dynein, we tracked the stepping of GST–dynein homodimers labeled with a single Qdot 655 placed on either the tail domain (through an N-terminal HaloTag; **Figs. 1a** and **2a–e**) or on a single motor domain (through a C-terminal HaloTag; see **Fig. 1a** and **Supplementary Fig. 2e–j**)[5]. Our new method of analysis revealed that the two-dimensional step size of tail-labeled dynein was ~10 nm (**Fig. 2b**), larger than the originally reported one-dimensional step size. However, when the two-dimensional data were projected onto the direction of motion along the microtubule axis, we observed an ~8-nm one-dimensional step size (**Fig. 2b**), in agreement with previous one-dimensional on-axis step sizes reported for dynein[5,7,22]. Observation of a fluorophore on a single motor domain (head-labeled) resulted in a two-dimensional step size of ~14–16 nm, whereas the one-dimensional on-axis step size was slightly smaller (**Supplementary Fig. 2i**). As reported previously, we found that the majority of dynein steps were in the forward direction (**Fig. 2c** and **Supplementary Fig. 2j**).

Analysis of the two-dimensional stepping data allowed us to determine the step size and angle of dynein's off-axis steps for the first time. We found that 77% of steps are forward steps, and many steps taken by the tail-labeled dynein and the single motor domain–labeled dynein contained an off-axis component > 6 nm (**Fig. 2d** and **Supplementary Fig. 2g**), unlike most kinesin-8 steps, which behaved similarly to other kinesins[30,31] (**Supplementary Fig. 2c**). The percentage of off-axis steps observed here was higher than previously reported[5], most likely owing to our development and implementation of the two-dimensional stepping algorithm, which allows a more accurate and thorough classification of the off-axis component of dynein stepping. However, both the curvature of the microtubule and the geometry associated with the distance between the fluorophore on the dynein motor domain and dynein's microtubule-binding domain could introduce additional sources of error for measurements in the off-axis direction. Thus, distances measured in the off-axis direction may be an underestimate and dynein may take more frequent and larger off-axis steps than we can detect.

© 2012 Nature America, Inc. All rights reserved.

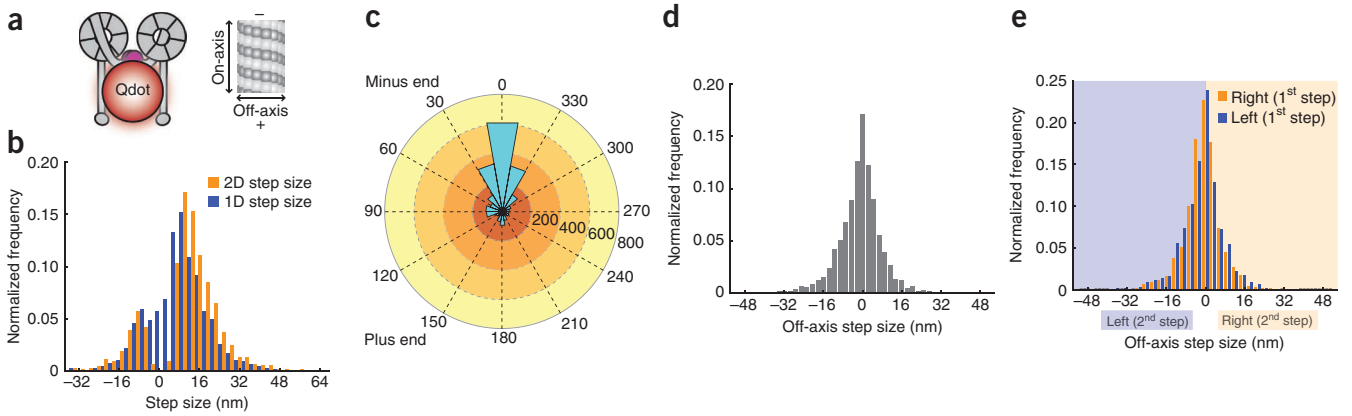

Figure 2 Two-dimensional stepping analysis of GST–dynein homodimers. (**a**) Schematic of a GST–dynein homodimer labeled with a Qdot through an N-terminal (tail domain) HaloTag and a diagram of a microtubule showing on- and off-axis directions of movement. (**b**) Histograms of dynein's step sizes in one (1D) and two (2D) dimensions. $N = 1{,}391$ steps for all panels. (**c**) An angle histogram (or rose plot) of the step angles. The stepping angle is defined as the angle between the stepping vector and the direction of on-axis movement. Steps to the left or right of the direction of motion are between 0° and 180° or between 180° and 360°, respectively. Steps between 90° and 270° are backwards steps. (**d**) Histogram of off-axis step sizes. (**e**) Histograms of leftward or rightward steps after a previous left or right step. Leftward and rightward steps are shown as steps with negative and positive off-axis components, respectively.

The two-dimensional analysis also allowed us to investigate whether dynein has a preference for stepping to the left or right. We calculated the probability that an off-axis step is followed by another off-axis step in the same direction and found that tail-labeled dynein is equally likely to step to the left or the right (**Fig. 2e**), irrespective of the direction of a prior off-axis step. In summary, by analyzing dynein stepping in two dimensions, we have found that dynein's true step size is larger than the previously reported one-dimensional step size, that many steps contain an off-axis component and that steps are equally likely to be to the left or to the right.

Development of DNA–dynein heterodimers

To determine how dynein's two motor domains move processively, we examined the stepping behavior of each of dynein's motor domains independently. Our prior work used a rapamycin-mediated FKBP–FRB heterodimer[5]; however, this complex has lower affinity[32] than is desirable for creating robust and stable heterodimers at the low protein concentrations necessary for single-molecule experiments. Instead, we chose a DNA-based dimerization approach that achieves high affinity (subfemtomolar for a 21-base-pair duplex at 22 °C (ref. 33)) and combinatorial flexibility and that allows individual

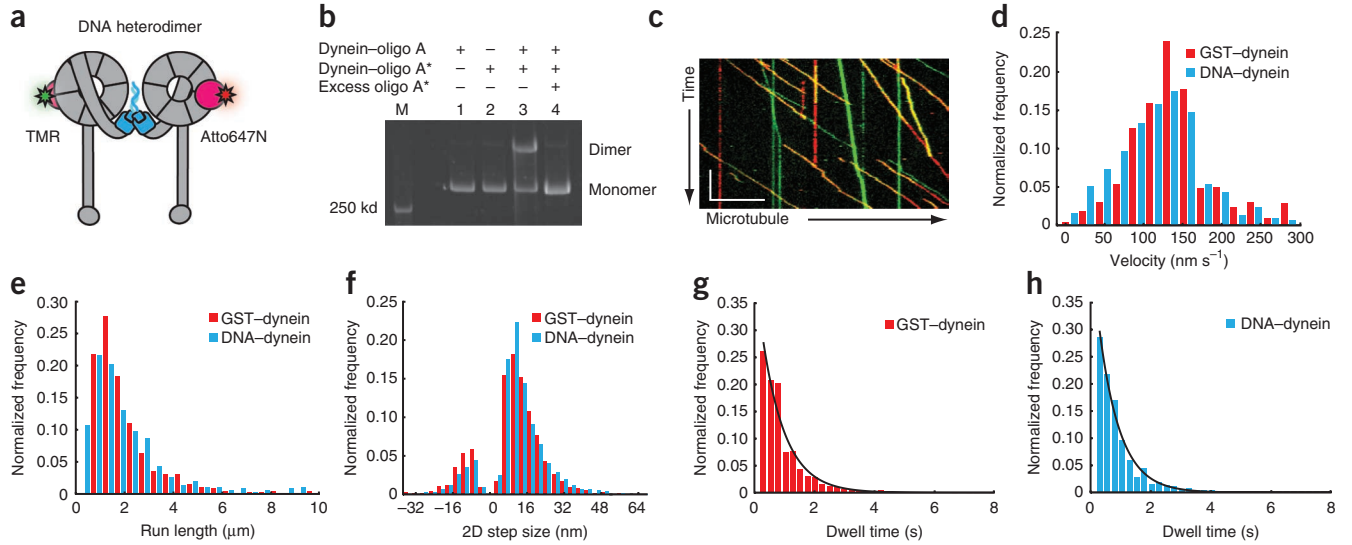

Figure 3 DNA-based dynein heterodimers are functional and step similarly to protein-based dynein homodimers. (**a**) Schematic of a DNA-based dynein heterodimer labeled with Atto647N (red star) and TMR (green star) through a C-terminal HaloTag (pink circles). The SNAP-tag and DNA oligomers (attached through the N-terminal SNAP-tag) are shown in blue. (**b**) LDS-PAGE gel showing dimerization of dynein monomers through DNA hybridization. Oligo, oligonucleotide. (**c**) Kymograph of the motility of DNA-based dynein dimers labeled with TMR (green) and Atto647N (red), with overlapping, dual-labeled heterodimers in yellow. Scale bars: *y*, 1 min; *x*, 10 μm. (**d**) Histograms of the velocity of GST- and DNA-based dynein dimers. (**e**) Histograms of the run length of GST- and DNA-based dynein dimers. (**f**) Histograms of the two-dimensional (2D) step size of GST- and DNA-based dynein dimers labeled with a single Qdot 655 on the N-terminal tail domain. (**g**,**h**) Histograms of the dwell time distribution of GST–dynein homodimers (**g**) and DNA–dynein heterodimers (**h**) labeled with a single Qdot 655 on the N-terminal tail domain. The distributions are fit to single exponential functions with stepping rates of $k = 1.78 \pm 0.13\ s^{-1}$ and $1.43 \pm 0.10\ s^{-1}$, respectively.

© 2012 Nature America, Inc. All rights reserved.

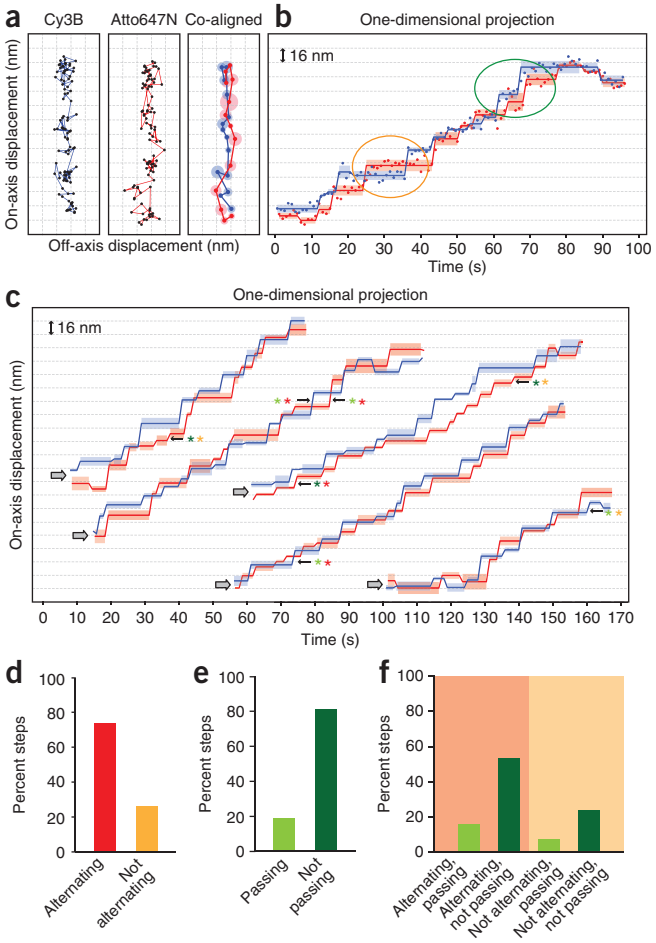

Figure 4 Two-color tracking of dynein stepping. (**a**) Representative two-color stepping trace of a DNA–dynein heterodimer. Left and center panels, raw two-dimensional positions (black dots in left and center panels) from a DNA–dynein heterodimer labeled with Cy3B and Atto647N. Right panel, co-alignment of the motor domain traces from each channel. Darker blue (Cy3B) and red (Atto647N) lines and dots represent steps determined by a two-dimensional step finding algorithm; larger, lighter-colored blue and red circles represent the s.d. of individual steps. (**b**) One-dimensional on-axis projection of the two-dimensional data from **a**, with lighter blue and red bars representing the s.d. of individual steps. Ovals highlight examples of hand-over-hand (orange) or inchworm (green) steps. The *y*-axis grid lines are spaced 16 nm apart in all panels. (**c**) Examples of one-dimensional on-axis projections of two-color stepping trace pairs from dual-labeled DNA–dynein heterodimers colored the same as in **b**. Grey arrows, start of each trace. Light green and red asterisks, alternating and passing steps (hand-over-hand); dark green and red asterisks, alternating and not passing steps ('inchworm'); light green and light orange asterisks, not alternating and passing steps; dark green and light orange asterisks, not alternating and not passing steps. (**d**) Temporal analysis of the relative frequency of stepping events. Alternating, current and previous stepping events originating from different heads; non-alternating, current and previous stepping events originating from the same head. $N = 268$. (**e**) Spatial analysis of the relative frequency of passing or not passing stepping events. $N = 233$. (**f**) Combined temporal and spatial analysis of stepping events. $N = 135$.

modification of each protomer within the dimer[34]. We reasoned that the dynein molecule would be amenable to this method, because its dimerization interface shows great plasticity[5]. Furthermore, the DNA dimerization interface should be stable under load, as yeast dynein's maximum force generation has been measured to be ~7 pN (ref. 22), whereas 'unzipping' DNA requires a force of ~14 pN (ref. 35).

To make DNA-based dynein dimers, we engineered a dynein monomer fusion protein in which the SNAP-tag replaced the N-terminal dimerization domain of the endogenous dynein heavy chain (**Fig. 1a**,**b**). This dynein monomer is also fused to a HaloTag at the C terminus of the motor domain to enable fluorophore labeling (**Figs. 1a** and **3a**). Both the SNAP-tag and HaloTag are small enzymes that form covalent bonds with their substrates, which can be coupled to fluorophores, biotin or reactive chemical groups. Taking advantage of the flexibility of the SNAP-tag, we coupled the 5′ or 3′ end of complementary, 21-nucleotide DNA oligonucleotides to the SNAP substrate, benzylguanine, and the DNA–benzylguanine molecules were then mixed with purified, SNAP-tagged dynein monomers. We found that this dimerization method was highly specific, with dynein monomers attached to complementary oligomers forming stable dimers, but not in the presence of excess, competing oligomers (**Fig. 3b**, compare lanes 3 and 4).

To determine if DNA-dimerized dynein was functional, we compared its motility and stepping pattern to GST–dynein homodimers. Each dynein monomer was labeled with a different small organic fluorophore (TMR or Atto647N) through the C-terminal HaloTag prior to dimerization (**Fig. 3a**). Using TIRF microscopy, we found that the majority of moving motors were dual-labeled (**Fig. 3c**), and their velocities and run lengths were similar to GST–dynein homodimers (134 ± 60.4 nm s^{-1} (mean ± s.d.) and 1.06 ± 0.044 µm (mean ± s.e.m., $N = 943$) for GST–dynein; 125 ± 56.1 nm s^{-1} (mean ± s.d.) and 1.45 ± 0.063 µm (mean ± s.e.m., $N = 866$) for DNA–dynein). (**Fig. 3d**,**e**). As a more stringent test of functionality, we determined the two-dimensional step size and dwell-time distribution of DNA–dynein dimers by labeling their tail domains with a Qdot 655. Again, we found these parameters to be comparable to those of GST–dynein homodimers (**Fig. 3f**–**h**). Notably, the stepping behavior of DNA–dynein heterodimers was also similar to native yeast dynein analyzed at both rate-limiting and cellular ATP concentrations[5,22], a further indication that both the method of dimerization and the low ATP concentrations (to slow the speed of the motor) used in our experiments do not alter the dynein stepping behavior. Together, these results indicate that DNA–dynein heterodimers are an effective model system for dissecting the dynein stepping mechanism.

Dynein's stepping is distinct from kinesin and myosin

All dimeric processive myosin and kinesin motors studied to date achieve processive motility by alternating the position of their two motor domains in both space and time (hand-over-hand stepping). We sought to determine if dynein had a similar spatial and temporal pattern of stepping. To do so, we used our DNA-dimerization method to construct dynein heterodimers labeled with the bright fluorophores Cy3B and Atto647N, which are much smaller (~2 nm in size) than Qdots (typically > 15 nm, larger than a dynein motor domain) and thus unlikely to interfere with dynein's motion. Dual-labeled dynein motors were imaged using near-simultaneous, alternating-excitation, high-precision TIRF microscopy under rate-limiting ATP conditions. We located the centroid position of each fluorophore-labeled motor domain with high precision by applying a two-dimensional Gaussian fit to the data from each channel[36], allowing for a position measurement precision of ~3.5 nm in both the *x* and *y* directions for both the Atto647N and Cy3B channels (**Supplementary Fig. 1b**,**c**; see **Supplementary Methods**). To precisely colocalize the Cy3B and Atto647N data, we applied the single molecule high resolution colocalization (SHREC) method[37], which yielded a mean mapping error of ~4 nm in both the *x* and *y*

© 2012 Nature America, Inc. All rights reserved.

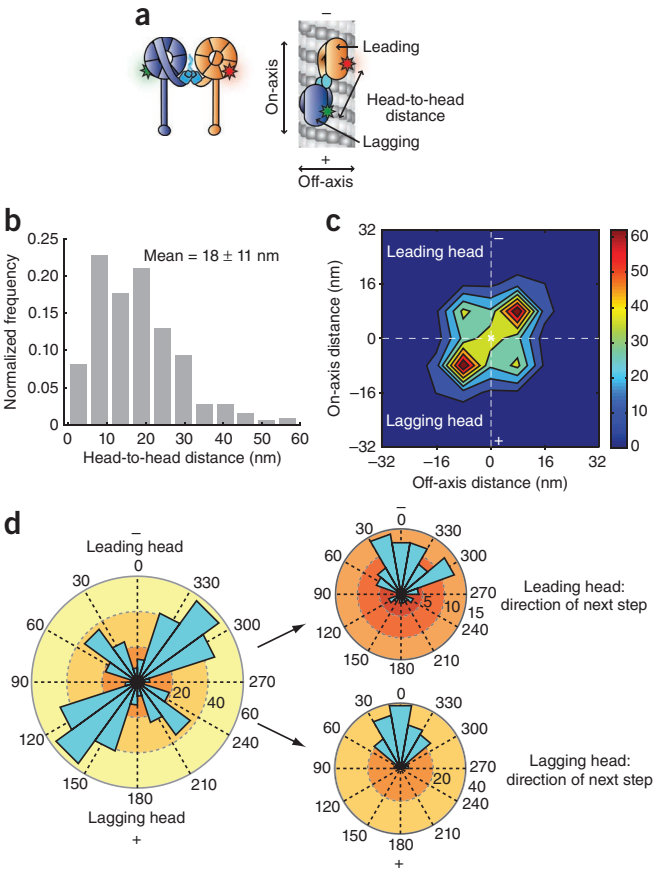

Figure 5 Spatial arrangement of dynein motor domains during the two-head-bound state. (**a**) Schematic of dual-labeled DNA-dimerized dynein bound to a microtubule. Other arrangements of the motor domains are possible. Fluorophores are represented by red and green stars. (**b**) Histogram of dynein's head-to-head distances during the two-head-bound state. $N = 523$. (**c**) Contour plot showing the left and right asymmetry between the leading and lagging heads. Orientation of the microtubule axis is vertical, as indicated by – and +, with the centroid position of each dynein molecule placed at the origin of the axes (white X). The number of occurrences of each position is indicated by the color bar on the right, with bin edges at 8-nm increments on both axes. $N = 256$ dimers or 512 heads. (**d**) Left, angle histogram of the position of the leading and lagging heads of individual dynein dimers relative to their respective centroid position (placed at the origin of the axes). Locations to the left or right of the direction of motion are between 0° and 180°, or 180° and 360°, respectively. $N = 256$ dimers or 512 heads. Right, angular distributions of the next step taken by the leading or lagging head. Steps between 90° and 270° are backwards steps.

directions and an overall uncertainty in our measurements of ~6 nm (**Supplementary Fig. 3a**,**b**; see **Supplementary Methods**).

Images from the Cy3B and Atto647N channels were screened for dual-labeled motile molecules with clearly defined two-dimensional stepping clusters (see **Supplementary Methods**). We analyzed 27 different two-color dynein stepping trace pairs, containing 708 steps (**Fig. 4a**,**b** and **Supplementary Fig. 3c–l**). The average one-dimensional, two-dimensional (compare **Supplementary Fig. 2i** with **Supplementary Fig. 3g**,**h**) and off-axis step sizes (compare **Supplementary Fig. 2g** with **Supplementary Fig. 3i**,**j**) were similar to the motor domain step sizes we observed for Qdot-labeled GST homodimers. Additionally, the one-dimensional on-axis step sizes (**Supplementary Fig. 3g**,**h**) we observed in each channel for the DNA–dynein were also very similar to those that we previously measured for full-length native yeast cytoplasmic dynein[5], another indication that the DNA-dimerization method is an effective model system for examining the dynein stepping mechanism.

Labeling each of dynein's two motor domains with different colored fluorophores allowed us to observe spatial and temporal relationships of the motor domains during processive motion (**Fig. 4a**,**b**; see **Supplementary Fig. 3c–f** for additional traces). Here we use the terms 'alternating' or 'not alternating' to describe the motor domains' relative temporal behavior and 'passing' or 'not passing' to describe their relative spatial behavior. The majority (~74%) of dynein steps alternated in time, but non-alternating events (a single head taking multiple steps in a row) were also observed (**Fig. 4b–d** and **Supplementary Fig. 3d**,**f**). In our spatial analysis of dynein stepping, we found that the majority (~83%) of dynein steps did not pass each other, although passing events (one head switching from the leading to the lagging position) were also observed (**Fig. 4b**,**c**,**e** and **Supplementary Fig. 3d**,**f**). These results (**Fig. 4f**) are in marked contrast to the well-studied two-headed processive kinesin and myosin motors, which show hand-over-hand stepping[26,27].

Spatial relationship of dynein's two motor domains

Despite recent reports of dynein's motor domain structure at near atomic resolution[18,20], the position and orientation of each motor domain within the dimer when bound to microtubules remain unknown. Therefore, we next determined the distance between dynein's motor domains in the 'two-head-bound state', when both heads were simultaneously bound to the microtubule (**Fig. 5a**,**b** and **Supplementary Fig. 4a–c**). As the dimensions of a dynein motor domain are ~12 nm (diameter of the AAA+ ring) by 10 nm (thickness of the AAA+ ring and linker) (**Fig. 1c**), our data suggest that the dynein motor domains are positioned close together. However, to accommodate the largest distances we observed between motor domains (4% of head-to-head distances were >30 nm), linker domain undocking from the motor domain probably occurs, a phenomena that has been observed in electron microscopy studies of both cytoplasmic and axonemal dyneins[10,12]. In addition, unlike other cytoskeletal motors, the distribution of head-to-head distances for dynein was broad and varied widely within individual traces (**Fig. 4a–c** and **Supplementary Fig. 3c–f**), further highlighting the unusual nature of dynein's stepping mechanism.

Our two-dimensional tracking of dynein stepping also allowed us to determine the spatial relationship of each dynein motor domain in the two-head-bound state relative to the direction of motion along the microtubule (**Fig. 5a**). In an analysis of motors with statistically resolvable (two-tailed Student's t-test with α 0.05) leading or lagging and left or right positions, we saw that the leading head was more likely to be to the right of the axis of motion, whereas the lagging head was more likely to be to the left of the axis of motion (**Fig. 5c**). This trend also extended to our entire dataset (**Supplementary Fig. 4d**). This suggests that the two motor domains of a dynein dimer do not typically reside on the same protofilament of a microtubule. These findings also imply that each dynein motor domain maintains a relatively stable identity of being a right-leading head or a left-lagging head. Although the dynein heads have a distinct left or right identity (64% of the leading heads are to the right of the microtubule axis), the direction of the next step taken by either a leading or lagging head is predominantly forward, with no off-axis bias (**Fig. 5d**), suggesting that dynein's two motor domains typically straddle at least one microtubule protofilament, but then move forward toward the microtubule's minus end.

© 2012 Nature America, Inc. All rights reserved.

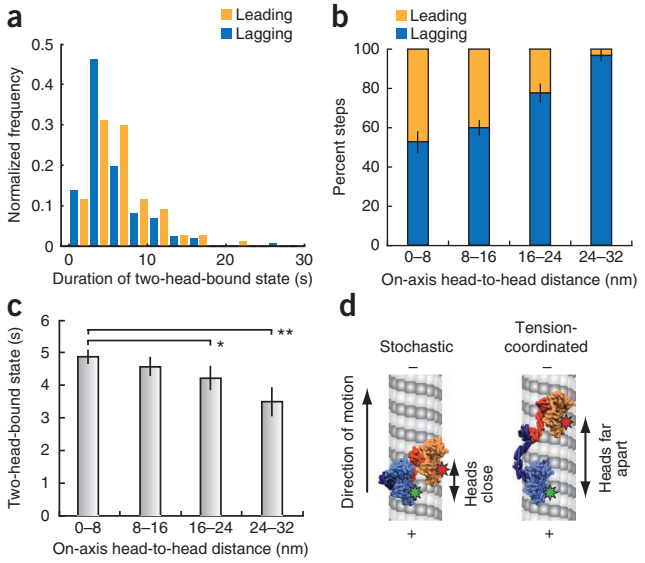

Figure 6 Dynein steps are stochastic at short head-to-head spacing and coordinated as head-to-head spacing increases. (**a**) Histograms of the duration of the two-head-bound states that are terminated by a leading-head stepping event or a lagging-head stepping event. (**b**) Relative stepping frequency of the leading and lagging heads as a function of the on-axis distance between motor domains. Error bars represent the s.e.m. and were generated by bootstrapping each bin. $N = 352$. (**c**) The duration of the two-head-bound state plotted as a function of the on-axis head-to-head distance. Mean durations ± s.e.m. are shown ($^{*}P = 0.0139$, $^{**}P = 0.0094$; two-tailed KS-test, alpha value 0.05, $N = 485$). (**d**) Model for the dynein stepping mechanism. The three-dimensional structure of dynein (PDB 3QMZ)[18], filtered to 8-Å resolution, was used to generate two microtubule-bound models of dimeric GST–dynein. The dynein rings are shown parallel to the long axis of the microtubule and parallel to each other, based on electron microscopy reconstructions[51–54]. Stepping is stochastic when dynein's motor domains are close together (left panel). Large distances between the two motor domains result in a tension-based mechanism that coordinates stepping (right panel).

Dynein's steps can be either stochastic or coordinated

The spatial asymmetry between the leading and lagging motor domains suggested that dynein's two heads have distinct identities when microtubule-bound. Additionally, optical trapping studies have shown that dynein responds asymmetrically to rearward and forward forces[22]. To determine whether tension had a role in dynein stepping, we analyzed the duration of two-head-bound states associated with leading- or lagging-head stepping events. The mean duration for two-head-bound states terminated by a lagging-head stepping (4.3 s, $N = 228$) is significantly shorter than that of two-head-bound states terminated by a leading-head stepping (5.4 s, $N = 119$, $P = 9.7 \times 10^{-5}$, alpha 0.05, one-tailed Kolmogorov-Smirnov (KS)-test, **Fig. 6a**). We hypothesized that the asymmetric response of leading and lagging heads is due to the difference in direction of the respective force vectors acting upon them along the microtubule axis.

Because motor domains separated by larger distances may experience increased tension, we examined whether dynein's stepping pattern changed as a function of the head-to-head distance. Dynein motor domains that were close together had an equal probability of the leading or lagging head stepping (**Fig. 6b**), but as the heads became separated by larger distances in the on-axis direction, the lagging head was increasingly more likely to step (**Fig. 6b**). This trend was also observable when we examined the duration of the two-head-bound state as a function of distance between motor domains in the on-axis direction. As larger distances separated the motor domains, the duration of the two-head-bound state decreased (**Fig. 6c**). Additionally, we found that the direction of the force is important for this effect, as neither the percentage of leading heads stepping versus lagging heads stepping nor the duration of the two-head-bound state varied as a function of the distance between motor domains, in the off-axis direction (**Supplementary Fig. 5a**,**b**).

Our results suggest that stochastic, uncoordinated stepping dominates when dynein's motor domains are close together, but when dynein's two motor domains are separated by larger distances, stepping becomes increasingly coordinated (**Fig. 6d**). We hypothesize that when large distances separate dynein's two motor domains, the dynein microtubule-binding domain may respond asymmetrically to force in the direction of movement along the microtubule (on-axis) but not across the microtubule (off-axis). This is consistent with reports that dynein responds asymmetrically to forward- and rearward-directed forces[22], as well as studies that demonstrate that dynein's step size is smaller under increased load[4,22].

DISCUSSION

A new model for the dynein stepping mechanism

By combining two-color, single-molecule microscopy with high-precision, two-dimensional tracking, we have shown that dynein's stepping mechanism is distinct from all cytoskeletal molecular motors characterized to date. Although many of dynein's steps alternate in time, most stepping events do not switch the leading or lagging spatial identities of dynein's two heads, a distinction from the two-headed processive myosin and kinesin motors that use alternating and passing (hand-over-hand) mechanisms. Strikingly, our data suggest dynein's steps are uncoordinated when the distance between motor domains is small, presumably because the intramolecular strain is low. However, as the distance between motor domains increases, our data show that dynein becomes increasingly coordinated, probably through a tension-based mechanism. These findings demonstrate that dynein is the first two-headed processive cytoskeletal motor to be identified that can alternate between stochastic- and tension-based stepping to achieve processivity (**Fig. 6d**).

In addition to the likelihood that tension may govern dynein's stepping behavior, the large size of the dynein motor domains (**Fig. 1c**) may impart steric constraints on the stepping pattern. Our data suggest that structural limitations influence the range and location of dynein on the microtubule lattice. We have found that dynein has an inherent left or right asymmetry, with the right motor domain of the dimer more likely to be the leading head and the left motor domain more likely to be the lagging head. It is unlikely that this asymmetry is generated by DNA-based dimerization, as the linkers we have included between dynein and the DNA contain multiple freely rotatable bonds. Therefore, a possible source of asymmetry could be the position of the linker domain, which lies across the face of the AAA+ ring and moves in response to the nucleotide occupancy at AAA1 (refs. 10,12). We propose that the linker domain of the motor on the right is 'sandwiched' between the dynein rings, whereas the linker domain of the motor on the left is not bound by another motor domain, imparting a structural and functional asymmetry (**Fig. 6d**). Our observation of large separations between dynein's two motor domains also suggests that the linker domain can undock from the motor domain (most likely the lagging motor, as shown in **Fig. 6d**, panel 2), as has been observed in electron microscopy studies of both cytoplasmic and axonemal dyneins[10,12].

The stochastic nature of dynein's stepping behavior raises the question of how a partially uncoordinated motor achieves processive

© 2012 Nature America, Inc. All rights reserved.

motility. In the case of kinesin-1, myosin-V and myosin-VI, processivity is accomplished by maintaining the leading head in a strong, filament-bound state until the lagging head detaches from the filament to pass the bound head and becomes the new leading head. Intramolecular tension between the motor domains provides a nucleotide gating mechanism that favors the detachment of the lagging motor domain and promotes a biased, diffusion-based search of this head for the next filament binding site[38–43]. It is possible that dynein's high duty ratio[21] substantially reduces the likelihood that both motor domains simultaneously dissociate from their microtubule track. This idea is corroborated by recent findings showing that mutant myosin-V and myosin-VI motors are still processive even when their tension-based gating mechanisms are impaired or destroyed[44,45]. However, our data do not rule out the possibility of nucleotide gating for dynein. For example, the fact that 74% of the steps we observed were alternating would be consistent with gating of some steps, as has been suggested by studies of *Dictyostelium* cytoplasmic dynein[46].

The similarity between the motility of the DNA–dynein heterodimer, the motility of the GST–dynein homodimer and that of native yeast dynein[5,22] suggests that the basic stepping mechanism will be the same for native dynein and the model systems that are currently being used to study the dynein mechanism. Thus, the DNA-based technique of heterodimer formation that we developed will be a powerful tool for orthogonal control over each dynein protomer for the study of additional heterodimer combinations in the future. However, our data do not rule out the possibility that dynein's native dimerization interface, associated subunits (intermediate, light intermediate and light chains), cofactors (dynactin, Lis1 and Nudel) or cargo may impart an additional layer of regulation on the dynein stepping mechanism. For instance, given that tension appears to coordinate dynein stepping, a compelling area for future study will be to determine if dynein's stepping mechanism becomes coordinated under the load of moving large cargo.

In vivo implications

Compared to other cytoskeletal motors, dynein's stepping behavior shows great variability and flexibility. Many dynein steps have an off-axis component; some steps are backwards, and dynein's two motor domains can step independently of each other. We propose that this flexibility allows dynein to navigate a crowded cytoplasm as well as obstacles on microtubules. Our results provide a molecular explanation for the observation that dynein is better able to navigate obstacles than are kinesin motors[47,48].

This apparent plasticity of the dynein stepping mechanism suggests that layers of regulation may be used to accomplish different cell biological functions. In eukaryotic cells, dynein transports dozens, if not hundreds, of different kinds of cargo, but there is only a single gene encoding cytoplasmic dynein 1 in all sequenced eukaryotic genomes (with the exception of flowering plants and some algae, which lack dynein genes[49,50]). Given the variability of the type, size and loads imparted by different cargo (ranging from endosomes to the mitotic spindle), a number of mechanisms for regulating cytoplasmic dynein's stepping behavior may have evolved. Future studies on the function of dynein-associated subunits and cofactors, on the effects of cargo load on motility, as well as on how multiple motors may coordinate to move cargo, will determine whether this partially uncoordinated motor is regulated to step coordinately for some functions.

METHODS

Methods and any associated references are available in the online version of the paper at http://www.nature.com/nsmb/.

Note: Supplementary information is available on the Nature Structural & Molecular Biology website.

ACKNOWLEDGMENTS

We thank X. Su and D. Pellman (Harvard Medical School) for providing purified kinesin-8; S. Zou for technical assistance; A. Carter, S. Churchman, A. Gennerich, Y. Goldman, A. Hendricks, J. Huang, A. Leschziner and A. Roberts for critical comments on the manuscript; F. Aguet, A. Besser, M. Vilela and G. Danuser for discussions of data analysis; M. Bagonis for early work on oligomer-SNAP linking; A. Leschziner for help with figure design; and A. Carter for providing MATLAB code. W.Q. is supported by a postdoctoral fellowship from the American Heart Association. S.L.R.-P. is funded by the Rita Allen Foundation, the Harvard Armenise Foundation and a US National Institutes of Health New Innovator award (1 DP2 OD004268-01).

AUTHOR CONTRIBUTIONS

W.Q. and N.D.D. contributed equally. W.Q., N.D.D., W.S. and S.L.R.-P. designed the experiments. W.Q., N.D.D. and B.S.G. conducted the experiments and analyzed the data. W.Q., N.D.D., B.S.G. and S.L.R.-P. wrote the paper. E.V. and D.W. wrote the two-dimensional particle tracking code.

COMPETING FINANCIAL INTERESTS

The authors declare no competing financial interests.

Published online at http://www.nature.com/nsmb/.
Reprints and permissions information is available online at http://www.nature.com/reprints/index.html.

1. Eschbach, J. & Dupuis, L. Cytoplasmic dynein in neurodegeneration. *Pharmacol. Ther.* **130**, 348–363 (2011).
2. Wynshaw-Boris, A. Lissencephaly and LIS1: insights into the molecular mechanisms of neuronal migration and development. *Clin. Genet.* **72**, 296–304 (2007).
3. King, S.J. & Schroer, T.A. Dynactin increases the processivity of the cytoplasmic dynein motor. *Nat. Cell Biol.* **2**, 20–24 (2000).
4. Mallik, R., Carter, B.C., Lex, S.A., King, S.J. & Gross, S.P. Cytoplasmic dynein functions as a gear in response to load. *Nature* **427**, 649–652 (2004).
5. Reck-Peterson, S.L. *et al.* Single-molecule analysis of dynein processivity and stepping behavior. *Cell* **126**, 335–348 (2006).
6. Ross, J.L., Wallace, K., Shuman, H., Goldman, Y.E. & Holzbaur, E.L. Processive bidirectional motion of dynein-dynactin complexes *in vitro*. *Nat. Cell Biol.* **8**, 562–570 (2006).
7. Toba, S., Watanabe, T.M., Yamaguchi-Okimoto, L., Toyoshima, Y.Y. & Higuchi, H. Overlapping hand-over-hand mechanism of single molecular motility of cytoplasmic dynein. *Proc. Natl. Acad. Sci. USA* **103**, 5741–5745 (2006).
8. Wang, Z., Khan, S. & Sheetz, M.P. Single cytoplasmic dynein molecule movements: characterization and comparison with kinesin. *Biophys. J.* **69**, 2011–2023 (1995).
9. Kardon, J.R. & Vale, R.D. Regulators of the cytoplasmic dynein motor. *Nat. Rev. Mol. Cell Biol.* **10**, 854–865 (2009).
10. Burgess, S.A., Walker, M.L., Sakakibara, H., Knight, P.J. & Oiwa, K. Dynein structure and power stroke. *Nature* **421**, 715–718 (2003).
11. Kon, T. *et al.* Helix sliding in the stalk coiled coil of dynein couples ATPase and microtubule binding. *Nat. Struct. Mol. Biol.* **16**, 325–333 (2009).
12. Roberts, A.J. *et al.* AAA+ Ring and linker swing mechanism in the dynein motor. *Cell* **136**, 485–495 (2009).
13. Vale, R.D. Switches, latches, and amplifiers: common themes of G proteins and molecular motors. *J. Cell Biol.* **135**, 291–302 (1996).
14. Gibbons, I.R. *et al.* Photosensitized cleavage of dynein heavy chains. Cleavage at the 'V1 site' by irradiation at 365 nm in the presence of ATP and vanadate. *J. Biol. Chem.* **262**, 2780–2786 (1987).
15. Cho, C., Reck-Peterson, S.L. & Vale, R.D. Regulatory ATPase sites of cytoplasmic dynein affect processivity and force generation. *J. Biol. Chem.* **283**, 25839–25845 (2008).
16. Kon, T., Nishiura, M., Ohkura, R., Toyoshima, Y.Y. & Sutoh, K. Distinct functions of nucleotide-binding/hydrolysis sites in the four AAA modules of cytoplasmic dynein. *Biochemistry* **43**, 11266–11274 (2004).
17. Silvanovich, A., Li, M.G., Serr, M., Mische, S. & Hays, T.S. The third P-loop domain in cytoplasmic dynein heavy chain is essential for dynein motor function and ATP-sensitive microtubule binding. *Mol. Biol. Cell* **14**, 1355–1365 (2003).
18. Carter, A.P., Cho, C., Jin, L. & Vale, R.D. Crystal structure of the dynein motor domain. *Science* **331**, 1159–1165 (2011).
19. Carter, A.P. *et al.* Structure and functional role of dynein's microtubule-binding domain. *Science* **322**, 1691–1695 (2008).
20. Kon, T., Sutoh, K. & Kurisu, G. X-ray structure of a functional full-length dynein motor domain. *Nat. Struct. Mol. Biol.* **18**, 638–642 (2011).
21. Shima, T., Imamula, K., Kon, T., Ohkura, R. & Sutoh, K. Head-head coordination is required for the processive motion of cytoplasmic dynein, an AAA+ molecular motor. *J. Struct. Biol.* **156**, 182–189 (2006).
22. Gennerich, A., Carter, A.P., Reck-Peterson, S.L. & Vale, R.D. Force-induced bidirectional stepping of cytoplasmic dynein. *Cell* **131**, 952–965 (2007).

© 2012 Nature America, Inc. All rights reserved.
npg

23. Gennerich, A. & Vale, R.D. Walking the walk: how kinesin and dynein coordinate their steps. *Curr. Opin. Cell Biol.* **21**, 59–67 (2009).
24. Sellers, J.R. & Veigel, C. Walking with myosin V. *Curr. Opin. Cell Biol.* **18**, 68–73 (2006).
25. Sweeney, H.L. & Houdusse, A. Myosin VI rewrites the rules for myosin motors. *Cell* **141**, 573–582 (2010).
26. Yildiz, A. *et al.* Myosin V walks hand-over-hand: single fluorophore imaging with 1.5-nm localization. *Science* **300**, 2061–2065 (2003).
27. Yildiz, A., Tomishige, M., Vale, R.D. & Selvin, P.R. Kinesin walks hand-over-hand. *Science* **303**, 676–678 (2004).
28. Samsó, M. & Koonce, M.P. 25 Angstrom resolution structure of a cytoplasmic dynein motor reveals a seven-member planar ring. *J. Mol. Biol.* **340**, 1059–1072 (2004).
29. Su, X. *et al.* Mechanisms underlying the dual-mode regulation of microtubule dynamics by Kip3/kinesin8. *Mol. Cell* **43**, 751–763 (2011).
30. Ray, S., Meyhofer, E., Milligan, R.A. & Howard, J. Kinesin follows the microtubule's protofilament axis. *J. Cell Biol.* **121**, 1083–1093 (1993).
31. Ray, S., Wolf, S.G., Howard, J. & Downing, K.H. Kinesin does not support the motility of zinc-macrotubes. *Cell Motil. Cytoskeleton* **30**, 146–152 (1995).
32. Banaszynski, L.A., Liu, C.W. & Wandless, T.J. Characterization of the FKBP. rapamycin.FRB ternary complex. *J. Am. Chem. Soc.* **127**, 4715–4721 (2005).
33. Markham, N.R. & Zuker, M. DINAMelt web server for nucleic acid melting prediction. *Nucleic Acids Res.* **33**, W577–W581 (2005).
34. Miyazono, Y., Hayashi, M., Karagiannis, P., Harada, Y. & Tadakuma, H. Strain through the neck linker ensures processive runs: a DNA-kinesin hybrid nanomachine study. *EMBO J.* **29**, 93–106 (2010).
35. Essevaz-Roulet, B., Bockelmann, U. & Heslot, F. Mechanical separation of the complementary strands of DNA. *Proc. Natl. Acad. Sci. USA* **94**, 11935–11940 (1997).
36. Thompson, R.E., Larson, D.R. & Webb, W.W. Precise nanometer localization analysis for individual fluorescent probes. *Biophys. J.* **82**, 2775–2783 (2002).
37. Churchman, L.S., Okten, Z., Rock, R.S., Dawson, J.F. & Spudich, J.A. Single molecule high-resolution colocalization of Cy3 and Cy5 attached to macromolecules measures intramolecular distances through time. *Proc. Natl. Acad. Sci. USA* **102**, 1419–1423 (2005).
38. Yildiz, A., Tomishige, M., Gennerich, A. & Vale, R.D. Intramolecular strain coordinates kinesin stepping behavior along microtubules. *Cell* **134**, 1030–1041 (2008).
39. Rosenfeld, S.S. & Sweeney, H.L. A model of myosin V processivity. *J. Biol. Chem.* **279**, 40100–40111 (2004).
40. Purcell, T.J., Sweeney, H.L. & Spudich, J.A. A force-dependent state controls the coordination of processive myosin V. *Proc. Natl. Acad. Sci. USA* **102**, 13873–13878 (2005).
41. Veigel, C., Schmitz, S., Wang, F. & Sellers, J.R. Load-dependent kinetics of myosin-V can explain its high processivity. *Nat. Cell Biol.* **7**, 861–869 (2005).
42. Sweeney, H.L. *et al.* How myosin VI coordinates its heads during processive movement. *EMBO J.* **26**, 2682–2692 (2007).
43. Dunn, A.R., Chuan, P., Bryant, Z. & Spudich, J.A. Contribution of the myosin VI tail domain to processive stepping and intramolecular tension sensing. *Proc. Natl. Acad. Sci. USA* **107**, 7746–7750 (2010).
44. Baboolal, T.G. *et al.* The SAH domain extends the functional length of the myosin lever. *Proc. Natl. Acad. Sci. USA* **106**, 22193–22198 (2009).
45. Elting, M.W., Bryant, Z., Liao, J.C. & Spudich, J.A. Detailed tuning of structure and intramolecular communication are dispensable for processive motion of myosin VI. *Biophys. J.* **100**, 430–439 (2011).
46. Numata, N., Shima, T., Ohkura, R., Kon, T. & Sutoh, K. C-sequence of the Dictyostelium cytoplasmic dynein participates in processivity modulation. *FEBS Lett.* **585**, 1185–1190 (2011).
47. Dixit, R., Ross, J.L., Goldman, Y.E. & Holzbaur, E.L. Differential regulation of dynein and kinesin motor proteins by tau. *Science* **319**, 1086–1089 (2008).
48. Ross, J.L., Shuman, H., Holzbaur, E.L. & Goldman, Y.E. Kinesin and dynein-dynactin at intersecting microtubules: motor density affects dynein function. *Biophys. J.* **94**, 3115–3125 (2008).
49. Lawrence, C.J., Morris, N.R., Meagher, R.B. & Dawe, R.K. Dyneins have run their course in plant lineage. *Traffic* **2**, 362–363 (2001).
50. Wickstead, B. & Gull, K. Dyneins across eukaryotes: a comparative genomic analysis. *Traffic* **8**, 1708–1721 (2007).
51. Ishikawa, T., Sakakibara, H. & Oiwa, K. The architecture of outer dynein arms *in situ*. *J. Mol. Biol.* **368**, 1249–1258 (2007).
52. Mizuno, N., Narita, A., Kon, T., Sutoh, K. & Kikkawa, M. Three-dimensional structure of cytoplasmic dynein bound to microtubules. *Proc. Natl. Acad. Sci. USA* **104**, 20832–20837 (2007).
53. Nicastro, D. *et al.* The molecular architecture of axonemes revealed by cryoelectron tomography. *Science* **313**, 944–948 (2006).
54. Ueno, H., Yasunaga, T., Shingyoji, C. & Hirose, K. Dynein pulls microtubules without rotating its stalk. *Proc. Natl. Acad. Sci. USA* **105**, 19702–19707 (2008).

© 2012 Nature America, Inc. All rights reserved.

ONLINE METHODS

Yeast strains. Modification of the endogenous *S. cerevisiae* dynein heavy chain gene was accomplished by insertion of the *Kluyveromyces lactis URA3* selectable marker into the *DYN1* gene at the location of the desired change. The *K. lactis URA3* gene was subsequently replaced with the SNAP-tag, SNAPf-tag (New England Biolabs), HaloTag (Promega) or GFP. Yeast strains used in this study are listed in **Supplementary Table 1**.

Preparation of HaloTag ligand–fluorophores. HaloTag ligand–fluorophore conjugates not commercially available were prepared as follows: Atto647N was conjugated to the HaloTag ligand by mixing 10 mM Atto647N NHS ester (Atto-Tec), 20 mM HaloTag–amine (O4) Ligand (Promega) and 30 mM N,N-diisopropylethylamine in dimethylformamide and nutating at 30 °C for 24 h. The HaloTag–Atto647N conjugate was separated from unreacted material by HPLC using a reverse-phase C18 column with a methanol: water gradient. Final product purity was > 85% as assessed by mass spectrometry. Cy3B–HaloTag was prepared by Bio-synthesis from Cy3B–NHS (GE Healthcare Lifesciences) and HaloTag–amine (O4) ligand (Promega).

Benzylguanine-conjugated DNA oligonucleotides. Benzylguanine-conjugated DNA oligonucleotides were prepared by mixing 10 mM benzylguanine–GLA–NHS (New England Biolabs) in anhydrous DMSO with 0.33 mM PAGE-purified amine- functionalized oligonucleotides (Bioneer) in 67 mM HEPES (pH 8.5) and 50% DMSO (v/v) for 30 min at 22 °C. Unreacted benzylguanine–GLA–NHS was removed using Micro Bio-Spin 6 Columns (Bio-Rad), pre-equilibrated with 10 mM Tris (pH 8.0), 150 mM KCl and 10% (v/v) glycerol. Linkage of benzylguanine to oligonucleotides was confirmed by gel shift assays on 20% TBE gels (Invitrogen). Oligonucleotide sequences used for dynein dimerization are listed in the **Supplementary Methods**.

Protein purification and labeling. Dynein motors were purified as described previously[5], with modifications detailed in the **Supplementary Methods**. Motors were labeled with benzylguanine-oligonucleotides and HaloTag ligand–fluorophores during dynein purification (see **Supplementary Methods**). Oligonucleotides used for labeling dynein and dynein monomers used in different experiments are listed in **Supplementary Table 2**.

TIRF microscopy. Motility assays were carried out using an inverted objective type Olympus IX-81 TIRF microscope with a 100× 1.45 N.A. oil immersion TIRF objective (Olympus) equipped with four continuous-wave diode-pumped solid state lasers: 405-nm and 640-nm cubic lasers (Coherent) and 491-nm and 561-nm lasers (Cobolt). Signals were detected with a back-thinned electron multiplier CCD camera (Hamamatsu). For near-simultaneous, two-color imaging, the microscope was modified to include a dual-band laser polychroic mirror (z561/635rpc, Chroma) and a dual-band sputtered emission filter (etCy3/Cy5m, Chroma) in the main optical path. The excitation path of the 561-nm laser was controlled by an acousto-optical tunable filter (NEOS; response time of 10 ms), and that of the 640 nm laser was controlled by a fast mechanical shutter (SmartShutter, Sutter; response time of 25 ms).

Stepping analysis. A custom program was written in MATLAB (Mathworks) to analyze dynein stepping behavior in both the temporal and spatial domains and determine correlated events. Briefly, all valid dwells included in the analysis were at least three frames long in their respective channels. A step was counted only if the dwells before and after contained at least three frames in that step's channel. Two-head-bound states were defined as containing three points or more (two in one channel and one in the other), where all points were part of a valid dwell location in their respective channels. Alternating and non-alternating steps were assigned only when both the current and previous steps were resolvable in time (that is, more than one frame away from each another). Leading or lagging identities were assigned only if the positions of both heads were different, as determined by a two-tailed Student's *t*-test with an alpha level of 5%. Position data are normally distributed about the mean, making a *t*-test appropriate. Classification of passing and not-passing steps was assigned only if the leading versus lagging identities before and after the step could be determined. See **Supplementary Methods** for details.

© 2012 Nature America, Inc. All rights reserved.